

Geometry and inclination of the broad line region in blazars

R. Decarli^{1*}, M. Dotti² and A. Treves³

¹Max-Planck-Institut für Astronomie, Königstuhl 17, 69117 Heidelberg, Germany

²Max-Planck-Institut für Astrophysik, Karl-Schwarzschild-Str. 1, D-85748 Garching, Germany

³Dipartimento di Fisica e Matematica, Università dell’Insubria, via Valleggio 11, I-22100 Como, Italy

ABSTRACT

We study the properties of the broad line region in blazars by comparing the virial estimate of black hole masses with that derived from the mass of the host galaxies. The former is sensitive to the width of broad lines, i.e., to the projection of the velocity of line-emitting clouds along the line of sight; the latter is not. This comparison allows us to constrain the deprojection factor f , thus revealing general properties of the geometry of the broad line region. We show that blazars tend to have 1) higher f values than the quasars of our reference sample: $\langle f_{\text{BL Lacs}} \rangle = 6.9 \pm 2.3$, $\langle f_{\text{blazars}} \rangle = 5.6 \pm 1.3$ and $\langle f_{\text{quasars}} \rangle = 2.0 \pm 0.3$; 2) relatively narrow broad emission lines; 3) modest equivalent widths, as expected because of the occurrence of jet emission at very low inclination angles. In a disc-like sketch of the broad line region, these results indicate a pole-on view of a flat geometry in blazars. This consistently extends the orientation-dependent unified model of active nuclei to the geometry of the broad line region.

Key words: (galaxies:) BL Lacertae objects: general – (galaxies:) quasars: emission lines

1 INTRODUCTION

The estimate of black hole masses (\mathcal{M}_{BH}) in distant galaxies is feasible only in active galactic nuclei (AGN), where we can infer the dynamics of gas close to the black holes (BHs) through its bright continuum and line emission. A common practice for type-1 AGN (where broad emission lines are observed) consists in adopting the virial paradigm:

$$\mathcal{M}_{\text{BH}} = \frac{R_{\text{BLR}} v_{\text{BLR}}^2}{G} \quad (1)$$

where R_{BLR} and v_{BLR} are respectively the orbital radii and the velocity of the gas clouds in the broad line region (BLR), and G is the gravitational constant. The cloud velocity is usually inferred from the width of broad lines, assuming a deprojection factor f :

$$v_{\text{BLR}} = f \cdot \text{FWHM} \quad (2)$$

while R_{BLR} is derived from the continuum luminosity of the accretion disc (Kaspi et al. 2000, 2005, 2007; Bentz et al. 2009). This allows an estimate of \mathcal{M}_{BH} from single-epoch spectra: Shen et al. (2010) applied this technique to the huge spectroscopic sample of quasars in the Sloan Digital Sky Survey (SDSS), thus providing \mathcal{M}_{BH} for $\sim 100,000$ sources.

The virial technique suffers of a number of limitations. In particular, the deprojection value f is not known, and is strongly sensitive to the (unknown) geometry and orientation of the BLR. In the commonly assumed isotropic picture of the BLR, $\langle f \rangle = \sqrt{3}/4$ (Netzer 1990). Assuming instead a disc-like geometry (e.g., McLure & Dunlop 2001),

$$f = 0.5 \left[\left(\frac{H}{R} \right)^2 + \sin^2 \vartheta \right]^{-1/2}, \quad (3)$$

where H/R is the aspect ratio of the disc and ϑ is the angle between the normal to the disc and the line of sight. In the limit of geometrically thin discs, equation 3 reduces to $f = 0.5/(\sin \vartheta)$, ranging between 0.5 (edge-on discs) and ∞ (face-on discs). Taking into account the thickness of the disc, $f \rightarrow 0.5 (H/R)^{-1}$ when $\vartheta \rightarrow 0$. For disc-like BLRs, $\langle f \rangle \approx 1$ almost independently of H/R (Decarli et al. 2008a).

From an observational point of view, average values for f have been estimated by comparing the mean offset of \mathcal{M}_{BH} estimates based on different techniques. Onken et al. (2004) compared the \mathcal{M}_{BH} values expected from the $\mathcal{M}_{\text{BH}}-\sigma_*$ relation for a set of local type-1 AGN with those obtained from the FWHM of $\text{H}\beta$ through equation 1, finding $\langle f(\text{H}\beta) \rangle = 2.3^1$. Collin et al. (2006) repeated the same exercise for a

* E-mail: decarli@mpia.de

¹ The average value reported here has been recomputed to account for the different definition of f used in Onken et al. (2004).

larger set of objects, and found a dependence of $\langle f(\text{H}\beta) \rangle$ on the broad line width ($\langle f \rangle \approx 1.5$ for $\text{FWHM} < 2000$ km/s, $\langle f \rangle \approx 0.7$ for $\text{FWHM} > 6000$ km/s), which could be attributed to the Eddington factor or to the BLR orientation. Decarli et al. (2008b) expanded on the previous results by Labita et al. (2006), comparing virial estimates of \mathcal{M}_{BH} based on H β and C IV lines with those inferred from the host galaxy luminosities assuming the scaling in Bettoni et al. (2003). They found $\langle f(\text{H}\beta) \rangle \approx 1.6$, $\langle f(\text{C IV}) \rangle \approx 2.4$ and a strong dependence of f on the widths of broad lines, i.e., $f > 2$ values are found only in quasars with $\text{FWHM} < 5000$ km/s (see also La Mura et al. 2007, 2009). The different values of $\langle f \rangle$ for different broad emission lines can be explained by a different geometry of the corresponding emitting regions (see also Fine et al. 2008, 2010).

Decarli et al. (2008a) noticed that the claimed “black hole mass deficit” observed in Narrow-Line Seyfert 1 galaxies (NLS1s; see Grupe & Mathur 2004) disappears once a disc-like BLR is assumed. NLS1s show relatively narrow permitted lines ($500 \text{ km/s} < \text{FWHM} < 2000 \text{ km/s}$), small \mathcal{M}_{BH} with respect to the predictions from the \mathcal{M}_{BH} -host galaxy relations, and high Eddington ratios. Assuming that the BLR is flat and seen almost pole-on, from the statistics of NLS1s with respect to ‘normal’ Seyfert 1 galaxies we can infer the average f value for NLS1s. Interestingly, once corrected for this higher deprojection values, line widths yield to distributions of \mathcal{M}_{BH} and Eddington ratios almost indistinguishable from normal Seyfert 1 galaxies. The strong radio loudness with blazar-like properties observed in a large fraction of NLS1 (Yuan et al. 2008) and the recent detection of GeV emission in a handful of NLS1s (Abdo et al. 2009a,b) also reveal the presence of beamed emission almost aligned with the line of sight, supporting a pole-on picture of the central engine of these AGN.

Other indications supporting a flat geometry for the BLR come from 1) the anti-correlation between the width of broad emission lines and the “compactness” parameter defined from radio observations as the luminosity ratio between the core and the lobe emission in radio galaxies and radio-loud quasars (Wills & Browne 1986; Brotherton 1996; Vestergaard, Wilkes & Barthel 2000); 2) the dependence of the FWHM of broad lines on the Equivalent Width of the [O III] line (Risaliti, Salvati & Marconi 2010).

In order to test the flat geometry picture of the BLR, we here extend our previous studies to blazars. According to the unified model of AGN (Antonucci & Miller 1985; Urry & Padovani 1995), blazar jets (and specifically BL Lac objects) are expected to show small inclination angles with respect to the line of sight. If the BLR has a flat geometry with a rotational axis aligned to the jet, blazars should show relatively narrow FWHM of broad lines and high values of f . We exploit a newly defined recipe to estimate the radius of the BLR from the luminosity of broad lines (see also Vestergaard & Peterson 2006) in order to avoid the contamination from the jet light in the optical continuum emission. Our virial estimates of \mathcal{M}_{BH} are then compared to the estimates we have from the $\mathcal{M}_{\text{BH}}-\mathcal{M}_{\text{host}}$ relation in order to derive f .

This paper is organized as follows: In section 2 we present our sample. Our analysis is described in section 3, while in section 4 we present our observational results and compare them with expectations from simple BLR models.

Conclusions are drawn in section 5. Throughout the paper we will assume a concordance cosmology with $H_0 = 70$ km/s/Mpc, $\Omega_m = 0.3$ and $\Omega_\Lambda = 0.7$. Results from other papers are accordingly scaled to this cosmology.

2 THE SAMPLE

In order to perform our analysis, we require an estimate of the host galaxy luminosity and a characterization of the properties (flux, width) of at least one broad line. The blazar sample is mostly derived from the compilations by Scarpa et al. (2000), Kotilainen et al. (1998) and Nilsson et al. (2003). Few other sources are taken from Wurtz et al. (1996), Nilsson et al. (2009) and Decarli et al. (2010b). We select all the blazars with a reliable estimate of the host galaxy luminosity. We adopt published values of $M_{\text{R}}(\text{host})$ or convert available bands into R computing the k -correction through the Elliptical galaxy template by Mannucci et al. (2001). Out of this selection, we pick up only those objects with a broad line detected in an optical spectrum. Main data sources for the spectroscopy are the `zbllac` database² and the SDSS archive. For BL Lac and OJ287, we use the FWHM and flux values published by Capetti, Raiteri & Buttiglione (2010) and Nilsson et al. (2010) respectively. It turns out that the only two lines of interest are Mg II $_{\lambda 2798}$ and H α . The former is the only broad line observed at $0.5 < z < 1.6$. We preferred the latter rather than H β because it is $\sim 3\times$ brighter. The whole blazar sample consists of 18 objects.

In order to understand the role of orientation of the broad line region with respect to ‘normal’ quasars, we include a comparison sample of quasars from the data set presented in Decarli et al. (2010a,b). We consider only objects where the Mg II or H α lines have been fully covered in the observed wavelength range. The reference sample consists of 39 sources. Table 1 summarizes the objects in both samples.

3 DATA ANALYSIS

3.1 Measured quantities

With the only exception of BL Lac and OJ287, for which published values have been used (Capetti, Raiteri & Buttiglione 2010; Nilsson et al. 2009), the spectra of all the blazars and reference quasars have been fitted with the fitting tools developed by our group and presented in Decarli et al. (2010a) and De Rosa et al. (2010). Namely, in order to infer the continuum and line properties, we apply a multicomponent fit to the continuum emission (power-law + Fe II model), subtract it, and fit the residual with the sum of two Gaussian functions with the same peak wavelength (see Decarli et al. 2008b, 2010a; De Rosa et al. 2010). The iron emission is modelled through the Vestergaard & Wilkes (2001) template in the UV and our own spectrum of I Zw001 in the optical wavelengths, after removing main emission lines and convolving to a Gaussian profile to mimic the Doppler broadening. Free parameters in the continuum estimate are the slope and

² See <http://www.oapd.inaf.it/zbllac/>.

Table 1. The sample. (1) Source name. (2–3) Source coordinate in J2000. (4) Redshift. (5) Absolute rest-frame R -band magnitude of the host galaxy. (6) Adopted Mass to Light ratio, in solar units. (7) \mathcal{M}_{BH} derived from the host galaxy luminosity. (8) Reference for the host galaxy luminosity: a- Kotilainen et al. (1998); b- Scarpa et al. (2000); c- Nilsson et al. (2003); d- Wurtz et al. (1996); e- Decarli et al. (2010b); f- Nilsson et al. (2009).

Name	R.A.	Dec.	z	M_{R} (host) [mag]	\mathcal{M}/L [M_{\odot}/L_{\odot}]	$\log \mathcal{M}_{\text{BH}}(\text{ima})$ [M_{\odot}]	Ref.
(1)	(2)	(3)	(4)	(5)	(6)	(7)	(8)
<i>Blazars</i>							
PKS0403-132	04:05:34.0	-13:08:14	0.571	-21.3	0.60	8.3	a
PKS0405-123	04:07:48.5	-12:11:36	0.574	-23.1	0.60	9.0	a
PKS0420-014	04:23:15.8	-01:20:33	0.915	-24.5	0.51	9.5	a
PKS0426-380	04:28:40.4	-37:56:20	1.105	-23.2	0.44	8.9	b
PKS0521-36	05:22:58.0	-36:27:31	0.055	-22.4	0.78	8.9	b
OJ049	08:31:48.9	+04:29:39	0.174	-23.4	0.73	9.3	c
OJ287	08:54:48.9	+20:06:31	0.306	-22.0	0.68	8.7	d
3C273	12:29:06.7	+02:03:09	0.158	-22.8	0.74	9.1	e
1249+174	12:51:45.3	+17:11:18	0.644	-21.0	0.58	8.2	b
3C279	12:56:11.1	-05:47:22	0.538	-24.0	0.61	9.4	f
PKS1519-273	15:22:37.7	-27:30:11	1.297	-24.4	0.38	9.3	b
4C1460	15:40:49.5	+14:47:46	0.605	-24.3	0.59	9.5	c
3C345	16:42:58.8	+39:48:37	0.594	-25.5	0.60	10.0	e
3C371	18:06:50.7	+69:49:28	0.051	-22.6	0.78	9.0	c
PKS2131-021	21:34:10.3	-01:53:17	1.284	-22.8	0.39	8.7	b
BL Lac	22:02:43.3	+42:16:40	0.069	-21.9	0.78	8.7	b
PKS2201+04	22:04:17.6	+04:40:02	0.027	-21.6	0.79	8.6	b
PKS2345-167	23:48:02.6	-16:31:13	0.576	-24.4	0.60	9.6	a
<i>Reference quasar sample</i>							
PKS0000-177	00:03:22.0	-17:27:12	1.465	-24.5	0.33	9.3	e
SGP5:46	00:52:22.8	-27:30:03	0.955	-22.4	0.50	8.7	e
0054+144	00:57:09.9	+14:46:10	0.171	-22.9	0.74	9.1	e
PKS0100-270	01:02:56.3	-26:46:36	1.597	-23.4	0.30	8.9	e
0119-370	01:21:24.1	-36:50:02	1.320	-23.7	0.37	9.1	e
0133+207	01:36:24.4	+20:57:27	0.425	-22.8	0.65	9.0	e
0152-4055	01:54:20.1	-40:40:30	1.650	-23.4	0.29	8.8	e
PKS0155-495	01:57:38.0	-49:15:19	1.298	-24.4	0.38	9.3	e
PKS0159-11	02:01:57.1	-11:32:34	0.669	-22.3	0.57	8.7	e
PB6708	02:09:48.8	-00:43:36	0.868	-22.8	0.52	8.8	e
KUV03086-0447	03:11:04.7	-04:35:41	0.755	-23.7	0.55	9.2	e
US3828	03:18:25.6	+15:59:56	0.515	-22.6	0.62	8.9	e
PKS0348-120	03:51:11.0	-11:53:23	1.520	-24.8	0.32	9.4	e
PKS0349-14	03:51:28.6	-14:29:10	0.614	-25.2	0.59	9.9	e
PKS0402-362	04:03:53.8	-36:05:02	1.417	-24.8	0.34	9.5	e
PKS0414-06	04:17:16.7	-05:53:45	0.773	-25.0	0.54	9.7	e
PKS0440-00	04:42:38.6	-00:17:43	0.607	-23.3	0.59	9.1	e
0624+6907	06:30:02.5	+69:05:04	0.370	-24.6	0.66	9.7	e
PKS0710+11	07:13:02.3	+11:46:15	0.768	-25.6	0.54	10.0	e
MS07546+3928	07:58:00.0	+39:20:29	0.096	-22.0	0.77	8.8	e
MS0824.2+0327	08:26:52.9	+03:17:13	1.431	-23.8	0.33	9.1	e
MS08287+6614	08:33:17.9	+66:03:46	0.610	-22.9	0.59	9.0	e
PKS0838+13	08:40:47.6	+13:12:23	0.684	-23.1	0.57	9.0	e
US1867	08:53:34.2	+43:49:02	0.513	-25.8	0.62	10.1	e
TON392	09:12:17.8	+24:50:38	0.654	-23.4	0.58	9.1	e
MS09441+1333	09:46:52.0	+13:20:26	0.131	-23.3	0.75	9.3	e
1004+130	10:07:26.1	+12:48:56	0.240	-23.6	0.71	9.3	e
Z101733-0203	10:17:33.5	-02:03:07	1.343	-21.8	0.36	8.3	e
PKS1015-31	10:18:09.3	-31:44:14	1.346	-24.5	0.36	9.4	e
PKS1018-42	10:20:03.9	-42:51:30	1.280	-25.1	0.39	9.6	e
1150+497	11:53:24.4	+49:31:09	0.334	-23.4	0.68	9.2	e
1402+436	14:04:38.8	+43:27:07	0.320	-23.3	0.68	9.2	e
1444+407	14:46:45.9	+40:35:06	0.267	-22.3	0.70	8.8	e
PKSJ1511-10	15:13:44.9	-10:12:00	1.513	-23.5	0.32	8.9	e
HS1623+7313	16:22:16.8	+73:06:15	0.621	-22.2	0.59	8.7	e
MC2212+172	21:14:56.7	+17:29:23	0.878	-24.1	0.52	9.4	e
Q2225-403B	22:28:50.4	-40:08:27	0.932	-23.2	0.50	9.0	e
2247+140	22:50:25.3	+14:19:52	0.235	-23.0	0.71	9.1	e
Q2348-4012	23:51:02.1	-39:56:18	1.500	-22.1	0.32	8.4	e

Table 2. Results from spectroscopy. (1) Source name. (2) Line used to estimate \mathcal{M}_{BH} . (3) FWHM. (4) Line luminosity. (5) Power-law monochromatic luminosity at 3000 Å (for Mg II) or 5100 Å (for H α). (6) Line Equivalent Width. (7) \mathcal{M}_{BH} estimate based on the line luminosity and width. (8) Geometrical factor f . (9) Reference for the spectra: a- Decarli et al. (2010a); b- Sbarufatti et al. (2005); c- Sbarufatti et al. (2006a); d- SDSS archive; e- Nilsson et al. (2010); f- Labita et al. (2006); g- Pian, Falomo & Treves (2005); h- HST STIS archive; i- Sbarufatti et al. (2006b); j- Capetti, Raiteri & Buttiglione (2010).

Name	Line	FWHM [km/s]	$\log L_{\text{line}}$ [erg/s]	$\log \lambda L_{\lambda}$ [erg/s]	E.W. [Å]	$\log \mathcal{M}_{\text{BH}}(\text{spec})$ [M_{\odot}]	f	Ref.
(1)	(2)	(3)	(4)	(5)	(6)	(7)	(8)	(9)
<i>Blazars</i>								
PKS0403-132	Mg II	3451	43.86	45.77	47.5	8.6	0.6	a
PKS0405-123	Mg II	3933	44.49	46.40	14.6	9.0	0.9	a
PKS0420-014	Mg II	3607	43.92	45.83	18.8	8.7	2.2	a
PKS0426-380	Mg II	4419	42.76	44.67	3.0	8.3	1.7	b
PKS0521-36	H α	4657	41.71	42.94	51.9	7.2	7.0	c
OJ049	H α	2553	41.55	42.78	3.5	6.6	21.3	d
OJ287	H α	3710	41.83	43.06	0.5	7.1	5.6	e
3C273	Mg II	4074	43.88	45.79	22.4	8.8	1.4	f
1249+174	Mg II	3040	43.01	44.91	27.5	8.1	1.0	d
3C279	Mg II	6534	43.29	45.20	8.6	8.9	1.6	g
PKS1519-273	Mg II	1821	42.37	44.28	0.4	7.4	7.9	b
4C1460	Mg II	2697	41.86	43.76	1.1	7.5	9.6	d
3C345	Mg II	4628	42.77	44.68	13.5	8.4	6.0	a
3C371	H α	2333	42.83	44.07	14.9	7.4	6.5	h
PKS2131-021	Mg II	3668	42.61	44.52	2.5	8.1	1.7	i
BL Lac	H α	4600	41.59	42.82	9.9	7.2	6.1	j
PKS2201+04	H α	3556	40.61	41.84	18.8	6.3	15.0	c
PKS2345-167	Mg II	3068	43.40	45.31	20.3	8.3	3.9	a
<i>Reference quasar sample</i>								
PKS0000-177	Mg II	6475	43.74	45.65	19.9	9.1	1.0	a
SGP5:46	Mg II	3504	42.94	44.85	23.4	8.2	1.4	a
0054+144	H α	8635	42.53	43.76	399.0	8.3	2.4	a
PKS0100-270	Mg II	3384	44.22	46.12	15.5	8.8	0.9	a
0119-370	Mg II	6229	43.58	45.49	60.3	9.0	0.9	a
0133+207	Mg II	12408	43.72	45.62	77.4	9.7	0.4	a
0152-4055	Mg II	4924	43.91	45.82	31.1	9.0	0.7	a
PKS0155-495	Mg II	5395	43.81	45.72	50.9	9.0	1.2	a
PKS0159-11	Mg II	4140	44.17	46.08	26.4	8.9	0.7	a
PB6708	Mg II	3156	43.58	45.48	53.8	8.4	1.4	a
KUV03086-0447	Mg II	2441	43.94	45.84	19.0	8.4	2.4	a
US3828	Mg II	3779	43.95	45.85	47.2	8.7	1.1	a
PKS0348-120	Mg II	3699	43.92	45.83	27.3	8.7	1.8	a
PKS0349-14	Mg II	5841	44.21	46.12	21.6	9.2	1.9	a
PKS0402-362	Mg II	4619	44.19	46.10	17.8	9.0	1.3	a
PKS0414-06	Mg II	5732	44.38	46.29	45.7	9.3	1.5	a
PKS0440-00	Mg II	5585	43.29	45.20	23.7	8.8	1.3	a
0624+6907	Mg II	3989	44.50	46.40	24.5	9.0	2.0	a
PKS0710+11	Mg II	11759	44.30	46.21	37.7	9.9	1.0	a
MS07546+3928	H α	2126	43.52	44.75	362.7	7.8	3.1	a
MS0824.2+0327	Mg II	2812	43.76	45.66	29.6	8.4	1.7	a
MS08287+6614	Mg II	6403	43.54	45.44	32.8	9.0	0.9	a
PKS0838+13	Mg II	4383	43.42	45.32	132.1	8.6	1.4	a
US1867	Mg II	2693	43.64	45.55	27.2	8.3	7.7	a
TON392	Mg II	4899	44.34	46.25	31.5	9.2	0.9	a
MS09441+1333	H α	2564	43.12	44.35	344.6	7.7	6.2	a
1004+130	H α	6356	43.72	44.95	238.9	8.8	1.7	a
Z101733-0203	Mg II	2914	42.61	44.52	28.5	7.9	1.3	a
PKS1015-31	Mg II	3835	43.14	45.04	1001.3	8.4	2.5	a
PKS1018-42	Mg II	4105	44.18	46.09	34.8	8.9	1.8	a
1150+497	H α	3523	43.47	44.70	439.4	8.2	3.2	a
1402+436	H α	2556	43.01	44.24	249.5	7.6	6.1	a
1444+407	H α	2694	42.69	43.92	355.2	7.4	4.8	a
PKSJ1511-10	Mg II	3285	43.72	45.63	16.0	8.5	1.3	a
HS1623+7313	Mg II	3250	43.38	45.29	36.3	8.3	1.3	a
MC2112+172	Mg II	4221	43.28	45.19	38.2	8.5	2.3	a
Q2225-403B	Mg II	4479	43.22	45.13	48.2	8.5	1.4	a
2247+140	H α	2832	42.86	44.10	120.8	7.6	5.6	a
Q2249-4012	Mg II	2816	44.81	45.93	30.0	8.7	0.3	a

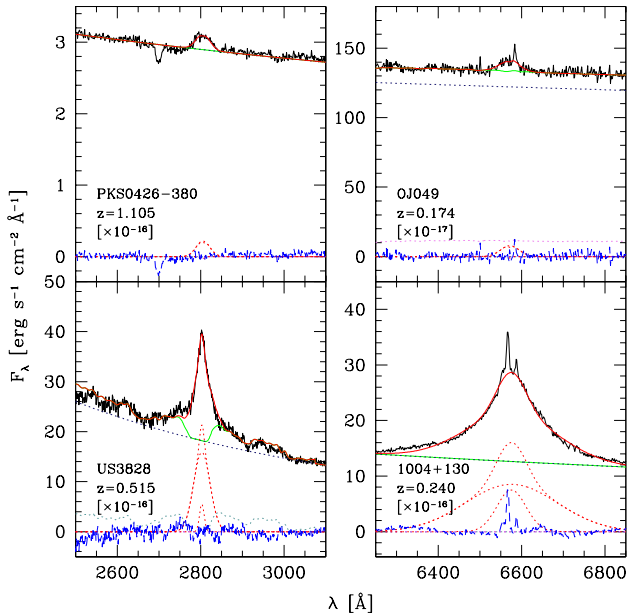


Figure 1. Examples of the continuum and line fits. The spectra of two blazars (PKS0426-380 and OJ049) and two quasars (US3828 and 1004+130) are shown. The solid black lines show the observed spectra, the solid red lines mark the model, which results from the superposition of a power-law continuum (dotted black lines), the iron and host galaxy templates (dotted light blue lines) and a line model (dotted red lines). The residuals after model subtraction are shown as blue dashed lines (a colour version of this plot is available in the electronic edition of the journal).

normalization of the power-law and the intensity of the Fe II feature. The iron multiplets are found to be negligible in the wavelength range bracketing H α . Two sources (PKS0521-36 and PKS2201+04) show significant emission from the host galaxy in their optical spectra. We modelled this component using the Elliptical template by Mannucci et al. (2001). According to our best fit, at 5100 Å, the host galaxies of these two objects account for $\sim 30\%$ of the specific flux. Two more objects (3C371 and OJ049) also show marginal ($\lesssim 5\%$ of the flux density at 5100 Å; see Figure 1) contribution from the host galaxies.

The line fit has 5 free parameters, namely the line peak, and the width and amplitude of the two Gaussian curves. Figure 1 shows four examples of fitting. From the line model we compute the Full Width at Half Maximum (FWHM), the integrated line flux (F_{line}), and the line Equivalent Width (EW). Following De Rosa et al. (2010), we compute uncertainties in the parameters by marginalizing the distribution of values yielding $\chi^2 < \chi^2_{\text{best}} + 1$. Fitting errors in the luminosities (both for the line and the continuum) are usually $\sim 5\%$, and never exceed 10%. Typical errors on the FWHM are $\sim 10\%$ (see also the analysis in Decarli et al. 2008b). We remark that these errors do not contribute significantly to the uncertainties on \mathcal{M}_{BH} and f , which are dominated by the scatter in the R_{BLR} -luminosity relations (~ 0.4 dex).

3.2 Derived quantities

The R_{BLR} -luminosity relations quoted above refer to the continuum emission of the accretion disc. This quantity is not directly accessible in blazars, where significant contamination from the synchrotron emission of the jet may occur. However, quasar spectra show a strong correlation between the luminosity of broad lines and the continuum luminosity of the accretion disc. This is not unexpected, as broad lines are emitted by gas directly photoionized by the continuum. Vestergaard & Peterson (2006) used the broad H β line luminosity as a proxy for the BLR radius in quasars. In the present case, this approach benefits of avoiding contaminations by the jet emission, hence representing a viable tool to estimate R_{BLR} even in blazars.

In Figure 2 we plot the continuum versus the broad line luminosities in quasars from Shen et al. (2010) for H α and Mg II. The latter shows a clear 1-to-1 correlation spanning several order of magnitudes. The average ratio between the continuum and the line luminosities is:

$$\log \frac{\lambda L_{\lambda}(3000\text{\AA})}{L_{\text{line}}(\text{MgII})} = 1.91 \pm 0.26 \quad (4)$$

where the error is the rms, and it was computed over 85515 quasars. Concerning H α , the scene is more complex. At low luminosities ($\lesssim 10^{44}$ erg/s in the continuum), significant contamination from the host galaxy is present. Bentz et al. (2009) showed that the removal of this contribution significantly improves the quality of the R_{BLR} -luminosity relation in the (rest frame) optical wavelengths. We therefore focus only on the bright end of the continuum luminosity distribution, where the role of starlight is negligible. A similar cut is also applied to the line luminosity, since fits of faint lines are less reliable due to the contaminations from narrow H α and [N II] lines. The average and rms values of the continuum to line luminosity ratios (computed over 1162 objects) is:

$$\log \frac{\lambda L_{\lambda}(5100\text{\AA})}{L_{\text{line}}(\text{H}\alpha)} = 1.23 \pm 0.14. \quad (5)$$

We used equations 4 and 5 to infer the disc contribution to the continuum luminosity. Since only one of the two lines can be observed in optical spectra (Mg II or H α , according to the target redshift), we adopted equation 4 for objects at $z > 0.5$ and equation 5 for the remaining sources.

Once the line width, luminosity and the (corrected) continuum luminosity are known, we use the R_{BLR} -luminosity relations by McLure & Jarvis (2002) and Kaspi et al. (2007) to compute \mathcal{M}_{BH} through equations 1–5. These estimates are compared with the \mathcal{M}_{BH} values we derive from the host galaxy. We convert host galaxy luminosities into masses by assuming that the stellar populations are old, generated in a single burst of instantaneous star formation at high- z (following Decarli et al. 2010b, we assume $z_{\text{burst}} = 5$), then passively evolving³. We adopt the mass-to-light ratio evolution predicted by Bruzual & Charlot (2003). The black hole mass

³ All the sources in our study have elliptical host galaxies (Scarpa et al. 2000; Nilsson et al. 2003; Decarli et al. 2010a). Therefore, we do not discriminate between the bulge and the whole galaxy. This is also consistent with the assumption of an old stellar population.

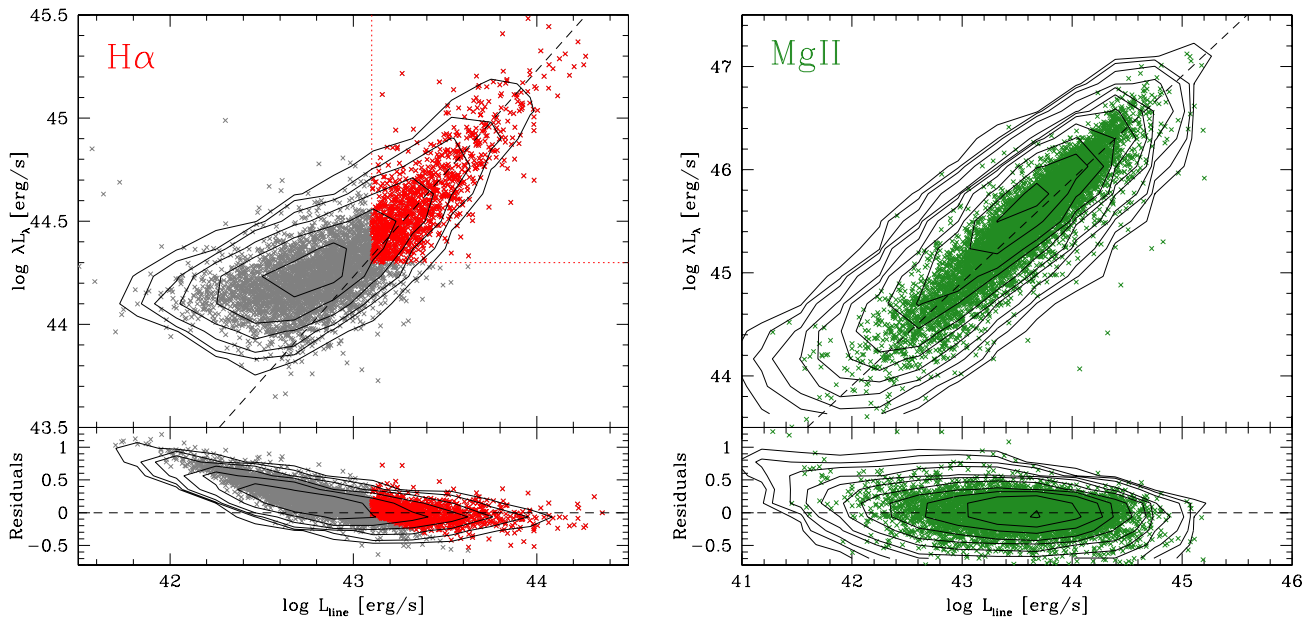


Figure 2. The continuum to line luminosity ratios for H α (*left panel*) and MgII (*right panel*). Data are taken from Shen et al. (2010). For the sake of clarity, in the MgII plots, only 1 object out of 5 is shown. Contours enclosing > 10, 20, 40, 80, . . . objects are also plotted. Dash lines show the average ratios. The plot region used to compute it for H α is marked with dotted lines. The faint end of the continuum luminosity distribution in the optical wavelengths is clearly deviating from the 1-to-1 relation, because of the contribution of the host galaxy starlight. The same is not true in the UV range, where the host galaxy contribution is negligible throughout the luminosity range of interest, and a clear linear correlation appears.

is then estimated through the (redshift-dependent) relation found in Decarli et al. (2010b):

$$\log \frac{\mathcal{M}_{\text{BH}}}{\mathcal{M}_{\text{bulge}}} = (0.28 \pm 0.06)z - (2.91 \pm 0.06) \quad (6)$$

We therefore can estimate f from the ratio between the image-based estimate of \mathcal{M}_{BH} and the one obtained from equation 1, using FWHM instead of v_{BLR} :

$$f = \sqrt{\frac{\mathcal{M}_{\text{BH}}(\text{image})}{\mathcal{M}_{\text{BH}}(\text{virial})}} = \sqrt{\frac{G\mathcal{M}_{\text{BH}}(\text{image})}{R_{\text{BLR}}\text{FWHM}^2}} \quad (7)$$

Tables 1 and 2 list the main measured and derived quantities for the blazar and reference samples.

4 RESULTS AND DISCUSSION

In Figure 3 we compare the \mathcal{M}_{BH} estimates obtained in the virial assumption, assuming $f = 1$, with the bulge mass inferred from the host galaxy luminosity. It is apparent that blazars, and specifically BL Lac objects, show smaller virial \mathcal{M}_{BH} values than quasars for a given host galaxy mass, i.e., higher values of f are required for blazars. We note that the redshift-dependent evolution of the $\mathcal{M}_{\text{BH}}/\mathcal{M}_{\text{host}}$ scaling relation has not been applied at this stage. The bulge mass range of blazars and quasars sampled in this study is the same, so no explicit bias due to the host galaxy is expected to affect our results. The same is true if we divide our sample according to the broad line width: No obvious segregation in terms of bulge mass is observed. Most importantly, when

we pick up pure BL Lac objects (with broad line Equivalent Width $\text{EW} < 10 \text{ \AA}^4$), we automatically select blazars among those showing the largest deviations between \mathcal{M}_{BH} and $\mathcal{M}_{\text{bulge}}$, as expected if we assume that BL Lac objects show the smallest inclination angles amongst blazars.

Figure 4 shows the f values as a function of the line FWHM. As already noted in Decarli et al. (2008b), an anti-correlation between f and FWHM is apparent. This supports the idea of a flat geometry viewed at different inclination angles. In particular, only few objects with $f > 2$ have $\text{FWHM} > 4000 \text{ km/s}$, and no one of them has $\text{FWHM} > 5000 \text{ km/s}$. It is also apparent that blazars have, on average, higher f than quasars. Namely, $\langle f_{\text{BL Lacs}} \rangle = 6.9 \pm 2.3$, $\langle f_{\text{blazars}} \rangle = 5.6 \pm 1.3$ and $\langle f_{\text{quasars}} \rangle = 2.0 \pm 0.3$, with all the BL Lac objects having $f \gtrsim 2$. All these indications support a flat geometry of the BLR, with smaller inclination angles for blazars and BL Lacs in particular.

Further evidence of this appears from the distribution of sources in the f -EW plane. As shown in Figure 2, the luminosity ratio between broad lines and continua is almost constant in the average quasar population (see also the analysis in Risaliti, Salvati & Marconi 2010). In BL Lac objects, the continuum emission from the jet contaminates the optical spectrum, so that the ratio between the line flux and

⁴ Here we slightly relaxed the usual $\text{EW} < 5 \text{ \AA}$ threshold in order to include BL Lac and 3C279. We note that, in order to study broad emission lines, we are biased towards spectra collected during relatively faint states of the continuum emission of BL Lac objects.

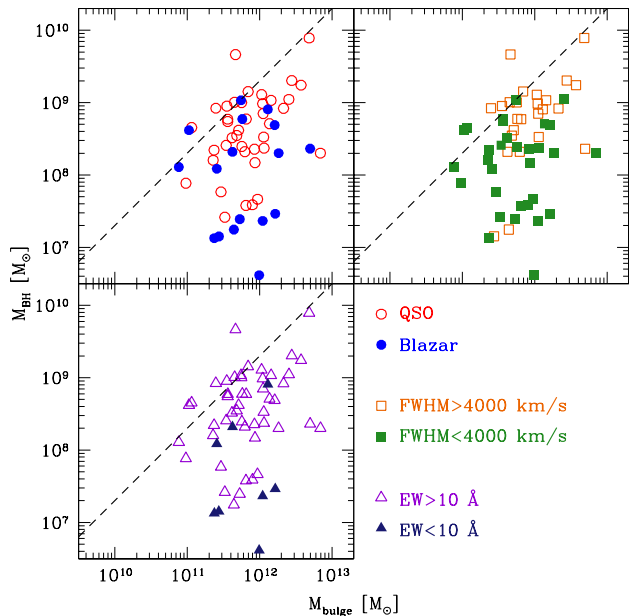


Figure 3. Comparison between black hole masses (derived through the virial technique, assuming $\text{FWHM} = v_{\text{BLR}}$) and the mass of the host galaxy bulge. The local Marconi & Hunt (2003) relation is plotted as dashed lines. Different symbols mark different subsamples: Filled / empty circles mark the blazars / reference quasars. Filled / empty squares mark objects with line width smaller / larger than 4000 km/s. Filled / empty triangles mark objects with EW below / exceeding 10 Å. Blazars (and BL Lac objects in particular) show smaller virial M_{BH} than expected from the host galaxy mass, i.e., larger f values.

the measured continuum (i.e., the line EW) is decreased. In Figure 5 we show that a) no quasar is found with small EW, as expected; b) the higher is f , the smaller is the EW. In particular, all the objects with $\text{EW} < 10$ Å have $f \gtrsim 2$. This picture is in good agreement with the expectations from the unified model of AGN if we assume a flat geometry for the BLR.

In order to put these results in the context of a quantitatively defined picture of the BLR, we compare the distribution of f observed in our study with the expectations from equation 3 through Montecarlo realizations. We generate a compilation of 10^5 objects with isotropically distributed inclination angles ϑ between the BLR rotational axis and the line of sight. We consider as pole-on systems those having $\vartheta < \vartheta_{\text{cut}} = 10^\circ$. The cutoff angle is set by the typical opening angle of a jet in BL Lac objects (see Ghisellini et al. 1993; Urry & Padovani 1995), i.e., we select sources in which we expect the jet to contaminate the continuum emission in the optical wavelengths. Objects with $\vartheta_{\text{cut}} < \vartheta < \vartheta_{\text{max}} \sim 40^\circ$ are considered normal type-1 AGN. The cutoff between these two classes is smoothed by adding an error $\sigma_\vartheta = 10^\circ$ to the intrinsic values of ϑ . This uncertainty accounts for errors in the estimate of f , intrinsic differences in the opening angles of the jets, and physical mis-alignment between the jets and the BLR rotational axis. This last effect is expected in a disc warped by, e.g., the Bardeen–Peterson effect (Bardeen & Peterson 1975).

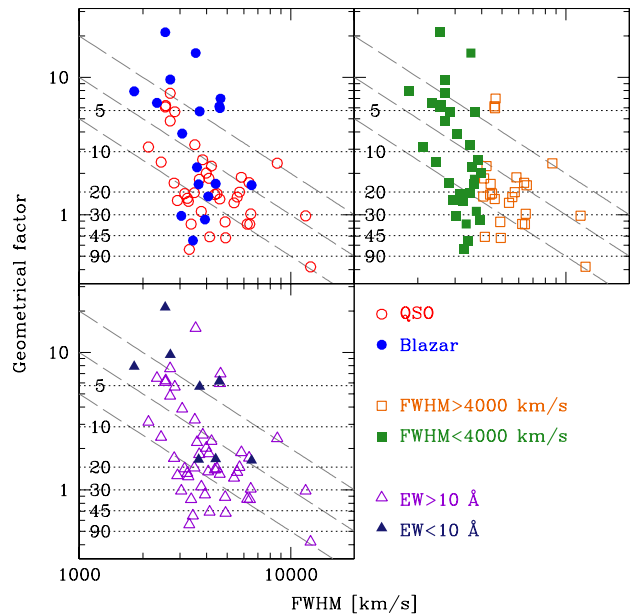


Figure 4. The geometrical factor f as a function of the width of the lines (FWHM). Dotted lines show the expected values of f for a thin disc model of the BLR, with different inclination angles (labelled in degrees). Diagonal, dashed lines mark the loci at fixed cloud velocities in the thin disc model, namely $v_{\text{BLR}} = 5000, 10000$ and 20000 km/s. Symbol code is the same as in Figure 3. Blazars (and specifically BL Lac objects) show relatively narrow lines and high f values, consistently with the picture of a flat BLR geometry observed pole-on.

In particular, for very massive BHs as those discussed here, the warping radius of a disc-like distribution of gas is comparable with the radius of the BLR (Perego et al. 2009). In this picture, an average misalignment of $\approx 10^\circ$ is expected if the BH is fuelled by a larger scale circumnuclear disc (Dotti et al. 2010). Other physical effects not considered here for sake of simplicity (e.g. self-irradiation driven warps, see Pringle 1996; Maloney, Begelman & Pringle 1996) could also play an additional role in smoothing the cutoff.

For each source we compute f through equation 3, and we compare the resulting distributions with what observed for objects with broad line Equivalent Width below 10 Å. Expected and observed distributions of f are shown in Figure 6, where we assumed $H/R = 0$. Despite the modest number of BL Lac objects, the agreement between the predicted and observed distributions is remarkably good. The Kolmogorov–Smirnov test indicates that the probability that the observed distribution of f for objects with $\text{EW} < 10$ Å is obtained by the same parent distribution that generated the pole-on sample in the Montecarlo realization is high (40%).

Concerning H/R , the observation of few, very-high values of f (> 10) suggests that, at least for these objects, $H/R \lesssim 0.05$. Re-running our Montecarlo realizations with $H/R = 0.05$ yields consistent results: In particular, the probability that the pole-on sample and the observed BL Lac objects have the same parent distributions is 20%.

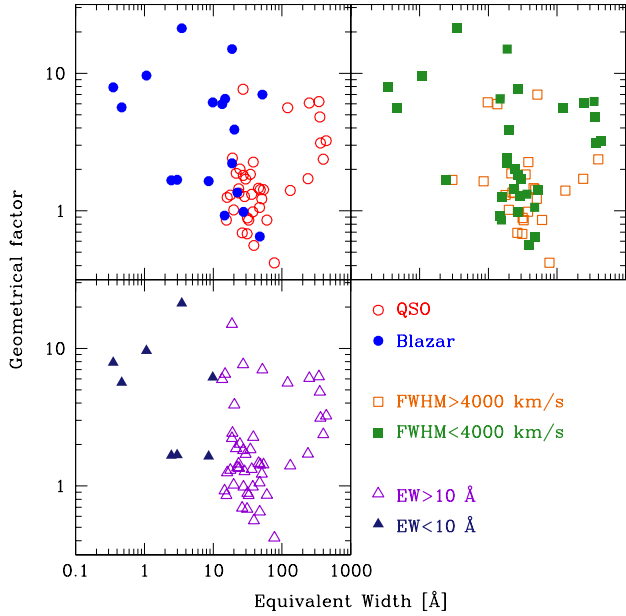


Figure 5. The geometrical factor f as a function of the Equivalent Width of broad lines. Symbol code is the same as in Figure 3. A trend is apparent, so that objects with strong jet contamination (= small line Equivalent Width) all present large geometrical factor values (consistent with a pole-on view of a flat geometry).

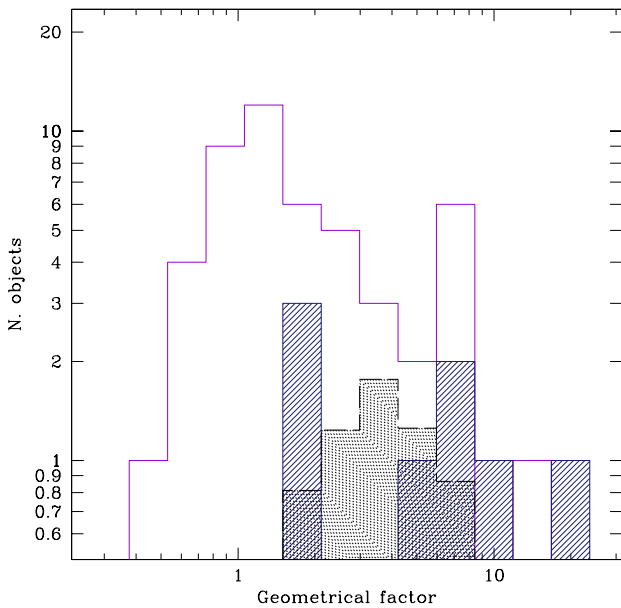


Figure 6. Observed distributions of the geometrical factor f for objects with broad line Equivalent Widths exceeding / below 10 Å (solid empty / shaded histograms), as compared with the output of our Monte Carlo realizations for pole-on sources (dotted shaded histogram; see the text for details). The agreement is remarkable, given the modest statistics of BL Lac objects in our sample.

5 CONCLUSIONS

We computed virial estimates of \mathcal{M}_{BH} in a set of 18 blazars and 39 reference quasars, and compared them with the \mathcal{M}_{BH} estimates derived from the host galaxy luminosities. Virial black hole masses are derived through broad line luminosities and widths, using a newly defined relation between the line and the continuum luminosity in quasars. From the comparison of the two \mathcal{M}_{BH} estimates we infer the geometrical factor f , responsible for the deprojection of the virial velocity from the line of sight, and we used f to constrain the properties of the broad line region in blazars. We found that:

i- Blazars, and BL Lac objects in particular, have higher f values on average with respect to the reference quasar sample, and both these classes have average f values well exceeding the predictions for an isotropic BLR. The average values of f for each class of objects are: $\langle f_{\text{BLLacs}} \rangle = 6.9 \pm 2.3$, $\langle f_{\text{blazars}} \rangle = 5.6 \pm 1.3$ and $\langle f_{\text{quasars}} \rangle = 2.0 \pm 0.3$.

ii- The geometrical factor clearly depends on the width of broad lines, in the sense that only few objects with $f \gtrsim 2$ have $\text{FWHM} > 4000$ km/s, and no one of them has $\text{FWHM} > 5000$ km/s. All the blazars in our sample have relatively narrow lines ($\lesssim 5000$ km/s).

iii- An anti-correlation between the geometrical factor and the broad line equivalent width is also found, in the sense that all the objects with $\text{EW} < 10$ Å have geometrical factors $f \gtrsim 2$.

These results rule out an isotropic sketch of the broad line region. The observed distribution of f is in excellent agreement with the expectations for a geometrically-thin ($H/R \lesssim 0.05$) disc picture. In this scheme, the broad line region of BL Lac objects is seen almost pole-on. Assuming small or negligible tilts ($< \text{few degrees}$) between the disc rotational axis and the AGN jet, this conclusion is in full agreement with the Unified Model of AGN.

ACKNOWLEDGMENTS

We are grateful to the Referee for his/her prompt feedback and fruitful comments. We thank G. Ghisellini for useful discussions.

REFERENCES

- Abdo A.A., Ackermann M., Ajello M., Axelsson M., Baldini L., Ballet J., Barbiellini G., Bastieri D., et al., 2009a, *ApJ*, 707, 727
- Abdo A.A., Ackermann M., Ajello M., Baldini L., Ballet J., Barbiellini G., Bastieri D., Bechtol K., et al., 2009b, *ApJ Letters*, 707, 142
- Antonucci R.R.J. & Miller J.S., 1985, *ApJ*, 297, 621
- Bardeen J. M., Petterson J. A., 1975, *ApJ*, 195, L65
- Bentz M.C., Peterson B.M., Netzer H., Pogge R.W., Vestergaard M., 2009, *ApJ*, 697, 160
- Bettoni D., Falomo R., Fasnano G. & Govoni F., 2003, *A&A*, 399, 869
- Brotherton M.S., 1996, *ApJS*, 102, 1
- Bruzual G., Charlot S., 2003, *MNRAS*, 344, 1000
- Capetti A., Raiteri C.M., Buttiglione S., 2010, *A&A*, 516, 59

- Collin S., Kawaguchi T., Peterson B.M., Vestergaard M., 2006, *A&A*, 456, 75
- Decarli R., Dotti M., Fontana M., Haardt F., 2008a, *MNRAS Letters*, 386, 15
- Decarli R., Labita M., Treves A., Falomo R., 2008b, *MNRAS*, 387, 1237
- Decarli R., Falomo R., Treves A., Kotilainen J.K., Labita M., Scarpa R., 2010a, *MNRAS*, 402, 2441
- Decarli R., Falomo R., Treves A., Labita M., Kotilainen J.K., Scarpa R., 2010b, *MNRAS*, 402, 2453
- De Rosa G., Decarli R., Walter F., Fan X., Jiang L., Kurk J., Pasquali A., Rix H.W., 2010, *ApJ* submitted
- Dotti M., Volonteri M., Perego A., Colpi M., Ruszkowski M., Haardt F., 2010, *MNRAS*, 402, 682
- Fine S., Croom S.M., Hopkins P.F., Hernquist L., Bland-Hawthorn J., Colless M., Hall P.B., Miller L., et al., 2008, *MNRAS*, 390, 1413
- Fine S., Croom S.M., Bland-Hawthorn J., Pimblett K.A., Ross N.P., Schneider D.P., Shanks T., 2010, *MNRAS*, accepted (arXiv:1005.5287)
- Ghisellini G., Padovani P., Celotti A., Maraschi L., 1993, *ApJ*, 407, 65
- Grupe D., Mathur S., 2004, *ApJ Letters*, 606, 41
- Kaspi S., Smith P.S., Netzer H., Maoz D., Jannuzi B.T., Giveon U., 2000, *ApJ*, 533, 631
- Kaspi S., Maoz D., Netzer H., Peterson B.M., Vestergaard M., Jannuzi B.T., 2005, *ApJ*, 629, 61
- Kaspi S., Brandt W.N., Maoz D., Netzer H., Schneider D.P., Shemmer O., 2007, *ApJ*, 659, 997
- Kotilainen J.K., Falomo R., & Scarpa R., 1998, *A&A*, 332, 503
- Labita M., Treves A., Falomo R., Uslenghi M., 2006, *MNRAS*, 373, 551
- La Mura G., Popović L.Č, Ciroi S., Rafanelli P., Ilić D., 2007, *ApJ*, 671, 104
- La Mura G., Di Mille F., Ciroi S., Popović L.Č, Rafanelli P., 2009, *ApJ*, 693, 1437
- Maloney P.R., Begelman M.C., Pringle J. E., 1996, *ApJ*, 472, 582
- Mannucci F., Basile F., Poggianti B. M. et al., 2001, *MNRAS*, 326, 745
- Marconi A., Hunt L.K., 2003, *ApJ Letters*, 589, 21
- McLure R.J., Dunlop J.S., 2001, *MNRAS*, 327, 199
- McLure R.J. & Jarvis M.J., 2002, *MNRAS*, 337, 109
- Netzer H., 1990, in *Active Galactic Nuclei*, ed. R. D. Blandford, H. Netzer, & L. Woltjer (Berlin: Springer), 137
- Nilsson K., Pursimo T., Heidt J., Takalo L.O., Sillanpää A., Brinkmann W., 2003, *A&A*, 400, 95
- Nilsson K., Pursimo T., Villforth C., Lindfors E., Takalo L.O., 2009, *A&A*, 505, 601
- Nilsson K., Takalo L.O., Lehto H.J., Sillanpää A., 2010, *A&A*, 516, 60
- Onken C.A., Ferrarese L., Merritt D., Peterson B.M., Pogge R.W., Vestergaard M., Wandel A., 2004, *ApJ*, 615, 645
- Perego A., Dotti M., Colpi M., Volonteri M., 2009, *MNRAS*, 399, 2249
- Pian E., Falomo R., Treves A., 2005, *MNRAS*, 361, 919
- Pringle J.E., 1996, *MNRAS*, 281, 357
- Risaliti G., Salvati M., Marconi A., 2010, *MNRAS* accepted (arXiv:1010.2037)
- Sbarufatti B., Treves A., Falomo R., Heidt J., Kotilainen J., Scarpa R., 2005, *AJ*, 129, 559
- Sbarufatti B., Falomo R., Treves A., Kotilainen J., 2006, *A&A*, 457, 35
- Sbarufatti B., Treves A., Falomo R., Heidt J., Kotilainen J., Scarpa R., 2006b, *AJ*, 132, 1
- Scarpa R., et al., 2000, *ApJ*, 532, 740
- Shen Y., Hall P.B., Richards G.T., Schneider D.P., Strauss M.A., Snedden S., Bizyaev D., Brewington H., et al. 2010, arXiv:1006.5178
- Urry C.M. & Padovani P., 1995, *PASP*, 107, 803
- Vestergaard M., Wilkes B.J., Barthel P.D., 2000, *ApJ*, 538L, 103
- Vestergaard M., Wilkes B.J., 2001, *ApJ Suppl.*, 134, 1
- Vestergaard M., & Peterson B.M., 2006, *ApJ*, 641, 689
- Wills B.J. & Browne I.W.A., 1986, *ApJ*, 302, 56
- Wurtz, Stocke & Yee, 1996, *ApJS*, 103, 109
- Yuan W., Zhou H.Y., Komossa S., Dong X.B., Wang T.G., Lu H.L., Bai J.M., 2008, *ApJ*, 685, 801

This paper has been typeset from a \TeX / \LaTeX file prepared by the author.